Structural Engineering and Mechanics, *Vol. 73, No. 6 (2020) 613-620*
DOI: https://doi.org/10.12989/sem.2020.73.6.613

Experimental study on all-bolted joint in modularized prefabricated steel structure

Zhanjing Wu*[1,2], Zhong Tao**[1], Bei Liu[1] and Heng Zuo[1]

[1]*School of Architecture Engineering, Kunming University of Science and Technology, Kunming 650500, China*
[2]*Post-doctoral Research Station of Mechanics, Kunming University of Science and Technology, Kunming 650500, China*

(Received July 29, 2019, Revised November 7, 2019, Accepted November 9, 2019)

Abstract. The research study is focuses on a form of all-bolted joint with the external ring stiffening plate in the prefabricated steel structure. The components are bolted at site after being fabricated in the factory. Six specimens were tested under cyclic loading, and the effects of column axial compression ratio, concrete-filled column, beam flange sub plate, beam web angle cleats, and spliced column on the failure mode, hysteretic behavior and ductility of the joints were analyzed. The results shown that the proposed all-bolted joint with external ring stiffening plate performed high bearing capability, stable inflexibility degradation, high ductility and plump hysteretic curve. The primary failure modes were bucking at beam end, cracking at the variable section of the external ring stiffening plate, and finally welds fracturing between external ring stiffening plate and column wall. The bearing capability of the joints reduced with the axial compression ratio increased. The use of concrete-filled steel tube column can increase the bearing capability of joints. The existence of the beam flange sub plate, and beam web angle cleat improves the energy dissipation, ductility, bearing capacity and original rigidity of the joint, but also increase the stress concentration at the variable section of the external reinforcing ring plate. The proposed joints with spliced column also performed desirable integrity, large bearing capacity, initial stiffness and energy dissipation capacity for engineering application by reasonable design.

Keywords: modularized prefabricated steel structure; all-bolted joint; external ring stiffening plate; quasi-static test; failure model

1. Introduction

The modularized prefabricated steel structure is assembled on site by factory-processed modules connected with high-strength bolts. Its benefits include rapid construction, less labor and pollution, belonging to a type of green and environment-friendly buildings (Lawson *et al*. 2012). It is widely used in developed regions such as Europe, the United States, Japan, and Australia, and will become one of the main forms of architectural development in China in the future. However, the welding of connection on site still affects the assembly speed (Fathieh *et al*. 2016). The reliability and safety of the beam-column joint are the prerequisites for ensuring the structural safety of the overall fabricated steel structure under normal use and disasters (Chen *et al*. 2004).

The box-column is widely used in prefabricated steel structure, due to the higher strength and same geometric and mechanical properties in both directions compared with H-section columns. Extensive study shows that the main connection method currently adopted is to install inner diaphragms (Shahidi *et al*. 2014).

The seismic performances of T-stub bolted joints have been studied (Swanson *et al*. 2000, Harada *et al*. 2007, Pilusoet *et al*. 2008, Popovet *et al*. 2002). Lee et al. investigated a new blind bolted joint to unfilled hollow section (HS) columns by cyclic loading test and FEA (Lee *et al*. 2011a, b. Lee *et al*. 2010). Shi *et al*. (2007), Dessouki *et al*. (2013) and Prinz *et al*. (2014) reported the seismic performance of a new beam-column joint with end-plate joints by static test and FEA.

The joints using inner diaphragms have the advantages of clear path for force transfer, large stiffness and high bearing capacity, but there are two problems affect the mounting speed: i) inner continuity plates are difficult to weld in the box-column and ii) difficult to transportation and erection.

Currently, other types of prefabricated modular beam-column joints have been suggested. A welded joint (Liu *et al*. 2017a), a bolted-welded joint (Liu *et al*. 2015), and an all-bolt joint (Liu *et al*. 2017b) were reported and the seismic function of those new modular prefabricated beam-column joints were also studied by static test and FEA. In the literature (Liu *et al*. 2017b), Liu *et al.* proposed a prefabricated modular joint connecting beam and column by combining the column flange with the all-bolted beam-column joint, and verified the feasibility of the joint via cyclic test, and proposed a simplified bearing capacity calculation formula. The results shown that such joints have excellent seismic function including ductility and energy dissipation capability due to bolted connections. Alifazl *et al*. (2018) conducted cyclic loading test on three

*Corresponding author, Professor
E-mail: zhanjing_wu@163.com
**Co-Corresponding author, Professor
E-mail: tsy0410@vip.sina.com

http://www.techno-press.com/journals/sem&subpage=7
ISSN: 1225-4568 (Print), 1598-6217 (Online)

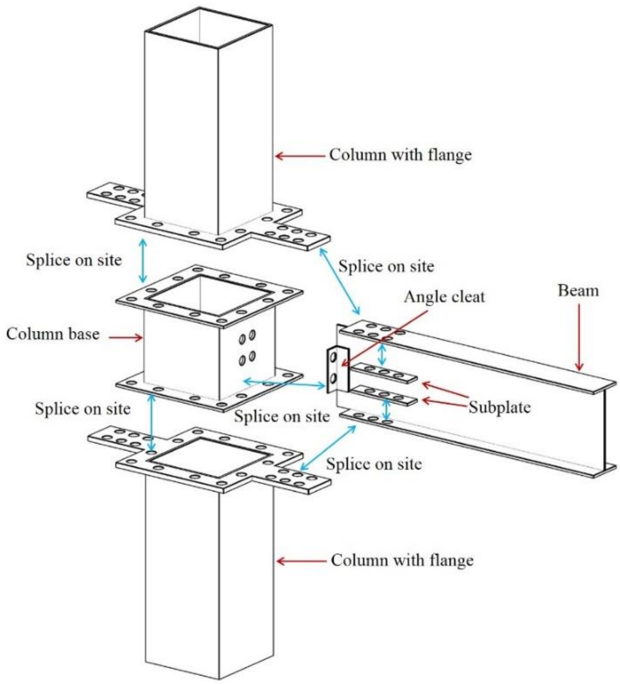

(a) Assembly drawing

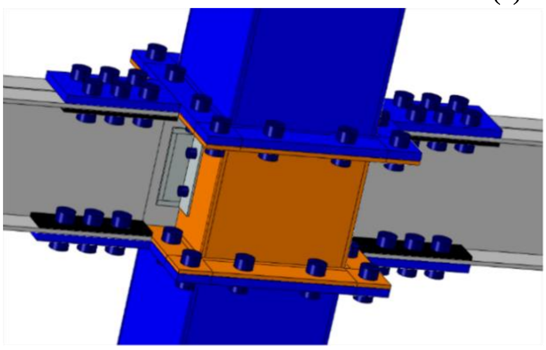

(b) Assembled joint

(c) Picture on site

Fig. 1 Structural diagram of the joint

prefabricated bolted beam-column joints, the effect of stiffness, ductility, and ultimate strength of the bolted joints with three different support shapes was evaluated. Deng *et al*. (2018) described a monotonic and quasi-static cyclic loading study on seven bolted connections with welded cover plates, and evaluated the seismic performance such as failure modes, ductility and energy dissipation capacity. Chen *et al*. (2017) reported an innovative design method of bolted connection between beams, and carried out cyclic loading test of six model specimens. The test results show that the stiffness and bearing capacity were increased and the ductility was reduced by using stiffeners. Other studies (Gholamiet *et al*. 2017, Hu *et al*. 2014, Wang *et al*. 2016, Mirghaderi *et al*. 2010) have also shown that all-bolted joint has adequate bearing ability and excellent energy dissipation capability.

In this paper, an innovative all-bolted beam-column joint with the external ring stiffening plate in the steel structure was proposed to improve the efficiency of prefabricated steel structure. The joints proposed in this paper connect prefabricated beams and columns together by using high-strength bolts and flanges, and can be rapidly assembled on site. Six full-scaled all-bolted beam-column joints with the external ring stiffening plate in the steel structure were constructed. The effects of the axial compression ratio, concrete-filled column, sub plate and web angle cleat on the seismic promance and failure mode of the joints were investigated.

2. Composition of the innovative joint

This study proposes an innovative modularized prefabricated all-bolted beam-column joint with the external ring stiffening plate, which mainly includes column with flange, column base with flange, subplate, angle cleat and H-shaped beam. The structural diagrams of the specimens are given in Fig. 1. As shown in Fig. 1, the external ring stiffening plate and the column, the column base and the flange, the beam and the angle cleat are prefabricated together in the factory, respectively. On site, the columns and the column base are spliced together via the external ring stiffening plate at the column end and the flange at the end of the column base; the columns and the beam flange

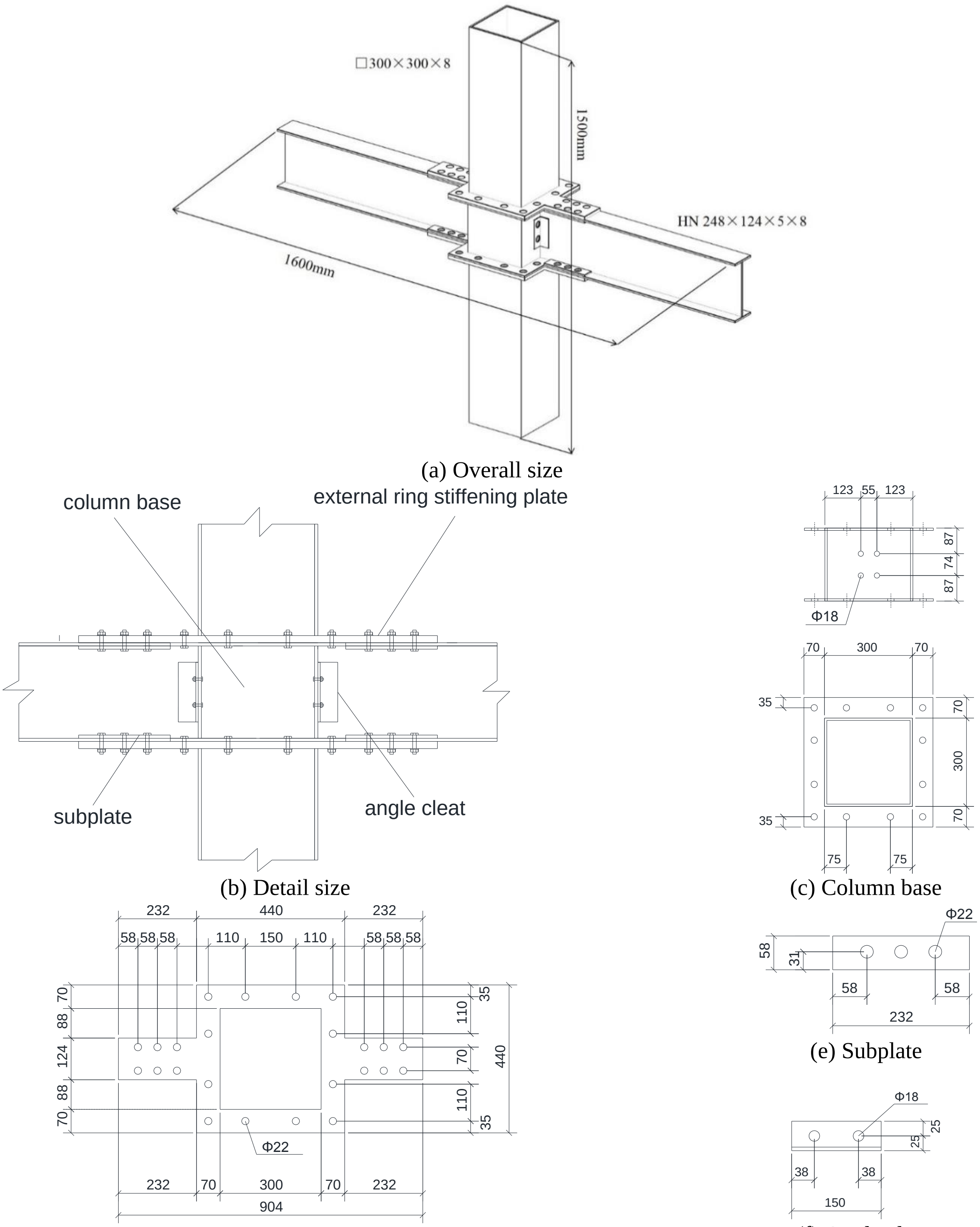

(a) Overall size

(b) Detail size

(c) Column base

(d) External reinforcing ring plat

(e) Subplate

(f) Angle cleat.

Fig. 2 Detail of specimens (Unit: mm)

were connected by the external ring stiffening plate and the high-strength bolts; Finally, the column base and the beam web were spliced together via the angle cleats and the high-strength bolts.

3. Experimental program

3.1 Test specimens

Six specimens were designed and manufactured, and in this experiment, the effect of axial compression ratios, concrete-filled column, angle cleat and sbuplate of joint mechanics were explored. Specimen SJ-2 changed the axial compression ratio to 0.6 based on SJ-1, and the effect of the ration from axial compression on seismic performance of joints were compared. SJ-3 poured concrete into the column based on JD1. JD4 canceled the subplates based on SJ-2. SJ-5 canceled angle cleats of the beam web based on JD1. SJ-6 used continuous column based on SJ-5. The primary design parameters of specimens are listed in Table 1.

The sizes of beam and column used in the test

Table 1 Design parameters of specimens

Specimen	Axial compression ratio	Angle cleat	Subplate	Column type	Concrete
SJ-1	0.3	√	√	splice	/
SJ-2	0.6	√	√	splice	/
SJ-3	0.3	√	√	splice	√
SJ-4	0.6	√	/	splice	/
SJ-5	0.3	/	√	splice	/
SJ-6	0.3	/	√	continuous	/

Table 2 Material properties

Steel type		f_y (Mpa)	f_u(Mpa)	E_s(Mpa)	$\varepsilon_y(10^{-6})$
Beam	flange	339.9	403.6	2.03×10^5	1790
	web	287.1	324.8	2.13×10^5	1262
Column		324.9	408.2	2.02×10^5	1752
External ring stiffening plate		348.6	424.8	2.03×10^5	1812

Note: f_y and f_u represent the yield and ultimate strength, respectively. ε_y denotes the strain corresponding to the yield strength. E_s is the Elastic modulus

specimens were taken from practical project. Q235B steel was used for all specimens. The profile of the box-column measures □300×300×8, the length of column was 1500 mm, the profile of the H-shaped steel beam measured HN248×124×5×8, and the length of beam was 1600 mm (symmetry at both ends of the beam); the angle cleat measured L150×50×50×4, and the subplate measured 232×58×8; The splicing bolts were all made of 10.9-grade friction type high-strength bolts (M20). The thickness of the external ring stiffening plate and flange plate were 16mm and 8mm, respectively. The concrete strength grade of the SJ-3 column was C30. The detailed diagram of the specimen is given in Fig. 2.

3.2 Material properties

The material properties are show in Table 2. The average compressive strength of concrete used in SJ-3 specimen was 23.35 MPa.

3.3 Test setup and loading scheme

Specimen tests were conducted at the Yunnan Institute of Engineering Earthquake Research. The experimental device is illustrated in Fig. 3. The specimen was placed in the loading frame to simulate the real stress state of the joint under the earthquake. The bottom of the column was hinged to the ground. The column top was installed with a hydraulic jack for controlling the axial compression ratio of the specimen. The low cyclic loading was applied on top of the loading frame by using a 1000kN hydraulic jack, and the specimens produced in-of-plane movement during the test.

The loading procedure is illustrated in Fig. 4, which including two loading steps: load-controlled and displacement-controlled. At the load-controlled phase, the lateral-loading increased by 10 kN per step and circulates once. At the displacement -controlled phase, the lateral-loading increased by 10 mm per step and circulates three times until the load dropped below 85% of the peak loading. During the loading procedure, the data were recorded automatically by a computer.

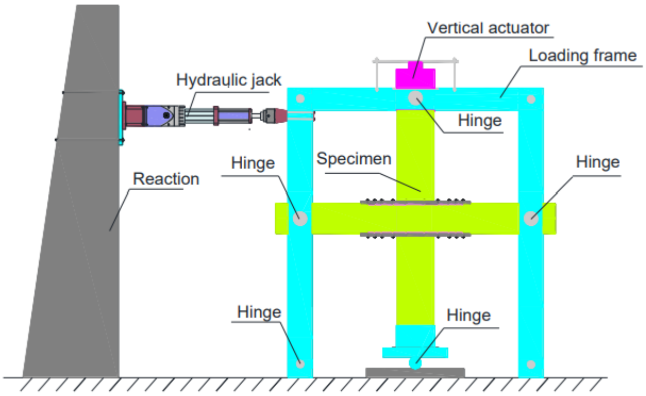

(a) Sketch of the test setup

(b) Photograph of the test setup

Fig. 3 Experimental setup

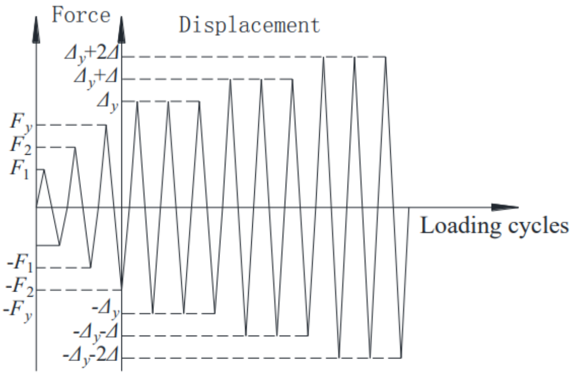

Fig. 5 Strain gauge layout

The strain gauge layout of specimens is shown in Fig. 5. Strain gauge and strain rosette of 3mm×2mm were arranged in the core area of joint, beam end, column end and the cross section of the reinforced ring plate. A displacement meter was placed between the beam end and the column end to measure the relative displacements. The load-displacement of column top was collected by a computer data system.

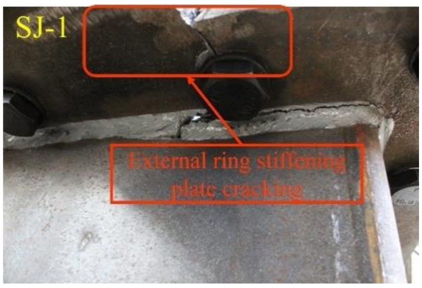

(a) External ring stiffening plate cracking of SJ-1

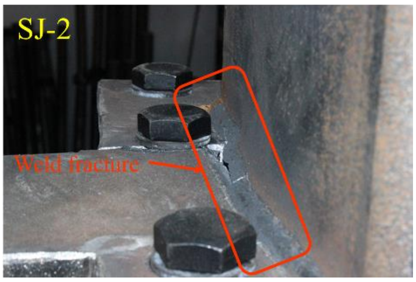

(b) Weld fracture of SJ-2

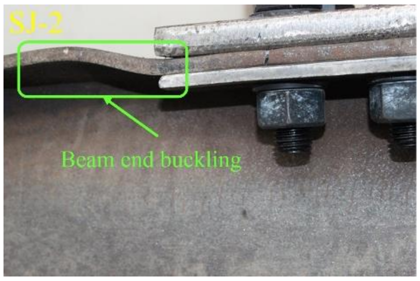

(c) Beam end buckling of SJ-2

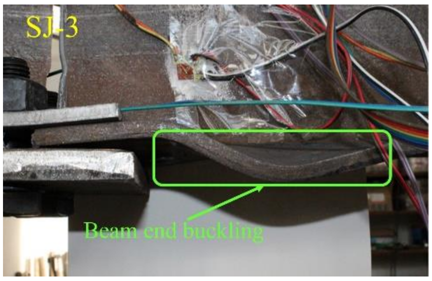

(d) Beam end buckling of SJ-3

(e) External ring stiffening plate cracking of SJ-3

(f) External ring stiffening plate cracking of SJ-4

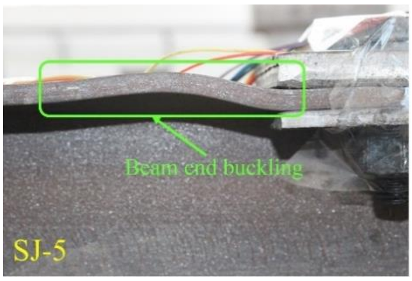

(g) Beam end buckling of SJ-5

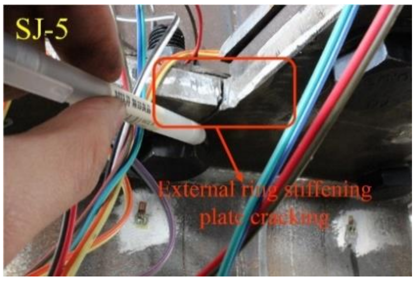

(h) External ring stiffening plate cracking of SJ-5

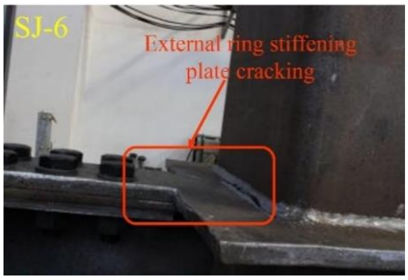

(i) External ring stiffening plate cracking of SJ-6

Fig. 6 Failure modes of specimens

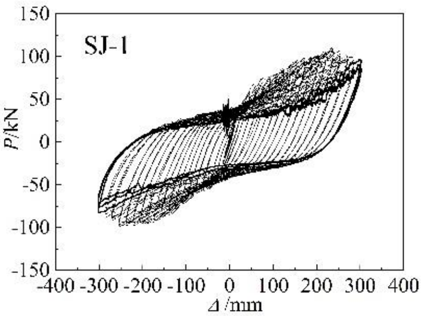

(a) Specimen SJ-1

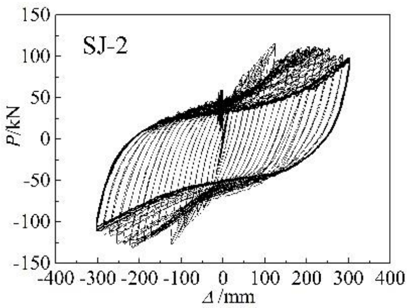

(b) Specimen SJ-2

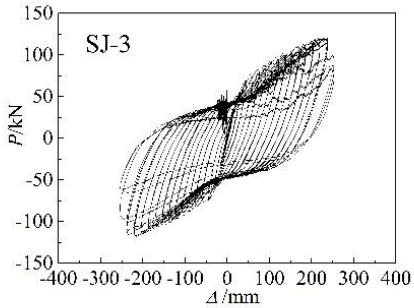

(c) Specimen SJ-3

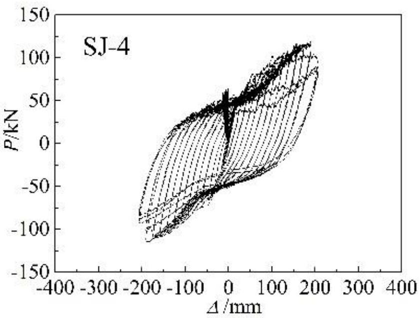

(d) Specimen SJ-4

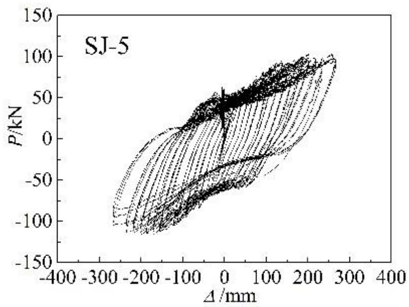

(e) Specimen SJ-5

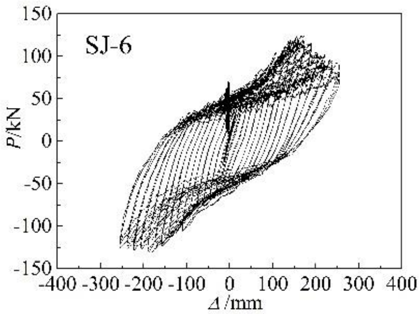

(f) Specimen SJ-6

Fig. 7 Load-displacement hysteretic curves of specimens

4. Experimental results and analysis

4.1 Experimental observations

At the initial stage of loading, no significant plastic deformation or fracture was observed in all specimens. Different failures occurred in each specimen as the loading displacement increased. The main failure modes are shown in Fig. 6.

All specimens began to deform plastically when the loading displacements reached approximately 32 mm - 48 mm. At approximately 80 mm - 96 mm, the beam flange began to exhibit bucking deformation. When the loading displacements reached approximately ±112 mm, slight cracks appeared at the variable cross-section of the external ring stiffening plate. The earliest cracks of all the external ring stiffening plates appeared at the variable section. As the loading displacements increased, cracks of the external ring stiffening plate developed to the weld at the joint between the external ring plate and the column end. With the loading process continuing, the bucking deformation of the beam flange developed rapidly. Finally, the cracks in the external ring stiffening plate continued to develop along the bolt hole to the weld of the column wall, leading to the tear of the weld seam.

The failure modes of the specimens were: the bucking deformation occurred at both beam and column end initiated prior to the tearing of the variable cross section of the external ring stiffening plate. The cracks gradually propagated away from variable cross section to the column wall with the loading increased. Finally, the weld seam between ring plate and column wall were torn under large loading displacement.

4.2 Load-displacement hysteretic curve

Fig. 7 shows the load-displacement hysteretic curves of the specimens. At initially loading, the load-displacement curves were linear. However, after loading, the residual deformation was small. With the loading process continuing, the hysteretic curve became plump. The slope decreased as the number of loading and unloading increases, indicating that the stiffness of specimen joints gradually degraded with loading. The main reason was the continuous accumulation of plastic deformation at beam ends and joints with the increase of the loading.

The hysteretic curve of specimen SJ-1 was plumper compared to SJ-2, indicating increased to axial compression ratio will decrease the energy dissipation capacity of the joint. The hysteretic curve of the specimen SJ-4 was relatively fuller than that of SJ-2, and specimen SJ-1 was fuller than that of SJ-5, because the deformation of the specimen with beam web angle cleats or subplates were more concentrated at beam end. The hysteretic curves of specimens SJ-5 and SJ-6 were similar, indicating that the spliced joint also had better energy dissipation capacity and integrity.

4.3 Skeleton curve

Fig. 8 shows the skeleton curve of the test joints. Under cyclic loading, the specimens experienced the process of elasticity, yielding, plastic deformation and ultimate failure.

At Initially loading stage, the column top load and displacement were linear, and the post-yield curve shown significant nonlinear characteristics. When the specimen entered the plastic stage, the bearing capacity of SJ-2 dropped rapidly, and the bearing capacity of SJ-1 was 12.49% higher than that of SJ-2. The ultimate bearing capability of specimen SJ-5 was higher compared to SJ-1, indicating that the existence of the beam web angle cleats improved the initial stiffness significantly and the bearing capability greatly of the joint. The ultimate bearing capability of SJ-6 (specimen with the continuous column) was 12.5% higher than that of SJ-5, but SJ-6 has more significant declining trend. It demonstrated that the joint using the spliced column also had good stiffness and bearing capacity.

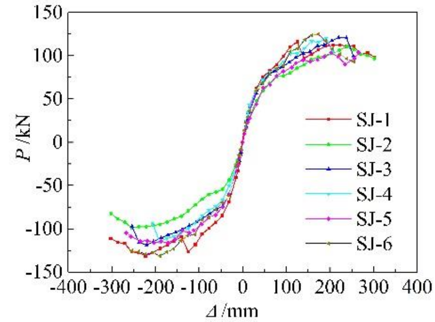

Fig. 8 Skeleton curves

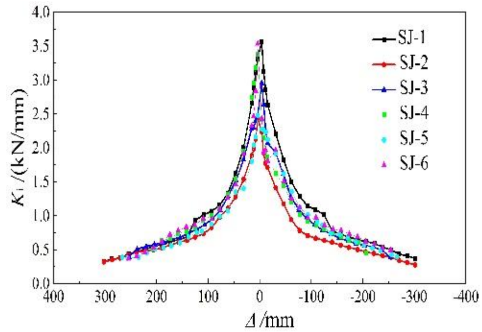

Fig. 9 Secant stiffness degradation curves

Table 3 Ductility and energy dissipation indexes of specimens

Specimen	Δ_y (mm)	Δ_u (mm)	μ	ζ_{eq}
SJ-1	84.70	300.69	3.55	0.24
SJ-2	111.06	302.08	2.72	0.20
SJ-3	93.46	251.41	2.69	0.21
SJ-4	98.67	266.41	2.70	0.20
SJ-5	98.67	266.41	2.70	0.20
SJ-6	112.32	254.45	2.65	0.21

4.4 Stiffness degradation

The secant stiffness degradation curve of specimens is shown in Fig. 9. The abscissa is the loading displacement, and the ordinate is the secant stiffness calculated according to Eq. (1).

$$K_i = \frac{|-F_i| + |+F_i|}{|-\delta_i| + |+\delta_i|} \tag{1}$$

where F_i and δ_i denote the i-th cyclic load peak and corresponding displacement, respectively. Fig. 9 show that the stiffness was significantly degraded with the loading increased. The stiffness degradation of specimen SJ-1 was less than that of SJ-2, indicating that excessive axial compression ratio can accelerate the stiffness degradation of joints. This phenomenon is consistent with the experimental results. The stiffness degradation rate of specimen SJ-1 was less compared to SJ-5, and SJ-1 has relatively large initial stiffness, indicating that the structure of beam web angle cleats was beneficial to reduce the stiffness degradation of joints and improved the initial stiffness of joints.

4.5 Ductility and energy dissipation capacity

The capabilities of ductility of specimens are characterized by displacement ductility coefficient μ. The displacement ductility coefficient of specimens can be calculated according to Eq. (2) (Xue *et al*. 2017).

$$\mu = \frac{\Delta_u}{\Delta_y} \tag{2}$$

where Δ_u is the ultimate displacement of the specimen, Δ_y is the yield displacement of the specimen. The energy dissipation capacity is the ability to absorb dissipated energy due to deformation of structural members under earthquake action. In this study, the equivalent viscous damping coefficient ζ_{eq} is used to evaluate the energy dissipation capacity of the specimen (Mirghaderi *et al*. 2010). The calculation results of the ductility and equivalent viscous damping coefficient of specimens are given in Table 3.

All specimens have displacement ductility coefficients of 2.65 - 3.55 and equivalent viscous damping coefficients of 0.2 - 0.24, indicating that all-bolted joint with the external ring stiffening plate in modularized prefabricated steel structure has good plastic deformation capacity and energy dissipation capacity. However, local tears of different degrees appeared in the external ring stiffening plate at the end of loading, which affected the ductility of the specimens, so it needed to be improved in practical engineering design. In general, the ductility coefficient of specimen SJ-1 was the largest, indicating that under a lower axial compression ratio, the all-bolted joint with the external ring stiffening plate can obtain better ductility by installing the beam web angle cleats and the subplates.

5. Conclusions

(1) The proposed all-bolted joint with the external ring stiffening plate in the prefabricated steel structure has sufficient ultimate bearing capacity and initial stiffness, plump hysteretic curve, with an average equivalent viscous damping coefficient of 0.21, indicating that the joint has excellent ductility and energy dissipation capability.

(2) The primary failure modes are cracks appeared at the variable cross section of the external ring stiffening plate, and developed towards near the bolt hole of the column base, and then developed to the weld between the external ring stiffening plate and the column wall. Finally, the weld seams between external ring stiffening plate and column wall were torn, and the beam flange exhibits a large plastic bucking deformation. The initial defects of the external ring stiffening plates have a great impact on the failure. Therefore, it is recommended to chamfer the variable section of the external ring plate during design, finish it at the factory for processing, and try to avoid the possible initial defects such as subtle irregularities and initial cracks of the base material at the initial variable section.

(3) The bearing capacity and energy dissipation capacity of joints can be improved by using concrete-filled steel tube column. However, compared with concrete-filled steel tube column joints, the proposed fabricated steel structure joints without pouring concrete also performed desirable bearing capacity and ductility for engineering application by reasonable design.

(4) The existence of the beam flange subplate and beam web angle cleat could improve the integrity and initial stiffness of the joint, so that the main deformation is more concentrated at the beam end. Meanwhile, the energy dissipation capacity, ductility performance and bearing capacity of the joints also can be improved. Although the phenomenon of stress concentration at the variable section of the external ring stiffening plate is more serious, it is still recommended to use these two components in such joints.

Acknowledgments

This work was supported by the National Key R&D Program of China (Grant No. 2017YFC0703600) and the National Natural Science Foundation of China (Grant No. 51668007). Financial support from the Technology and Yunnan Earthquake Engineering Researching Center for Zhanjing wu's work at the Post-doctoral Research Station of Mechanics of Kunming University of Science and Technology, as a postdoctoral researcher, is highly appreciated.

References

Azizi Naserabad, A., Ghasemi, M., Shabakhty, N. and Ghohani Arab, H. (2018), "Evaluation of three support shapes on behavior of new bolted connection BBCC in modularized prefabricated steel structures", *Int. J. Steel Struct.*, **18**(5), 1639-1653. https://doi.org/10.1007/s13296-018-0051-9.

Chen, C., Lin, C. and Tsai, C. (2004), "Evaluation of reinforced connections between steel beams and box columns", *Eng. Struct.*, **26**(13), 1889-1904. https://doi.org/10.1016/j.engstruct.2004.06.017.

Chen, Z., Liu, J. and Yu, Y. (2017), "Experimental study on interior connections in modular steel buildings", *Eng. Struct.*, **147**, 625-638. https://doi.org/10.1016/j.engstruct.2017.06.002.

Deng, E., Zong, L., Ding, Y., Dai, X., Lou, N. and Chen, Y. (2018), "Monotonic and cyclic response of bolted connections with welded cover plate for modular steel construction", *Eng. Struct.*, **167**(3), 407-419. https://doi.org/10.1016/j.engstruct.2018.04.028.

Dessouki, A., Youssef, A. and Ibrahim, M. (2013), "Behavior of I-beam bolted extended end-plate moment connections", *Ain Shams Eng. J.*, **4**(4), 685-699. https://doi.org/10.1016/j.asej.2013.03.004.

Fathieh, A. and Mercan, O. (2016), "Seismic evaluation of modular steel buildings", *Eng. Struct.*, **122**, 83-92. https://doi.org/10.1016/j.engstruct.2016.04.054.

Gholami, M., Deylami, A. and Tehranizadeh, M. (2013), "Seismic performance of flange plate connections between steel beams and box columns", *J. Constr. Steel Res.*, **84**, 36-48. https://doi.org/10.1016/j.jcsr.2012.11.011.

Harada, Y. and Morita, K. (2007), "Design of wide-flange section column-to-split-tee tensile connection with high-strength bolts", *J. Struct. Eng.*, **133**(3), 335-346. https://doi.org/10.1061/(asce)0733-9445(2007)133:3(335).

Hu, F., Shi, G., Bai, Y. and Shi, Y. (2014), "Seismic performance of prefabricated steel beam-to-column connections", *J. Constr. Steel Res.*, **102**, 204-216. https://doi.org/10.1016/j.jcsr.2014.07.012.

Lawson, M., Ray, O. and Rory, B. (2012), "Application of modular construction in high-rise buildings", *J. Arch. Eng.*, **18**(2), 148-154. https://doi.org/10.1061/(ASCE)AE.1943-5568.0000057.

Lee, J., Goldsworthy, H. and Gad, E. (2010), "Blind bolted T-stub connections to unfilled hollow section columns in low rise structures", *J. Constr. Steel Res.*, **66**(8-9), 981-992. https://doi.org/10.1016/j.jcsr.2010.03.016.

Lee, J., Goldsworthy, H. and Gad, E. (2011a), "Blind bolted moment connection to unfilled hollow section columns using extended T-stub with back face support", *Eng. Struct.*, **33**(5), 1710-1722. https://doi.org/10.1016/j.engstruct.2011.02.008.

Lee, J., Goldsworthy, H. and Gad, E. (2011b), "Blind bolted moment connection to sides of hollow section columns", *J. Constr. Steel Res.*, **67**(12), 1900-1911. https://doi.org/10.1016/j.jcsr.2011.06.007.

Liu, X. C., Pu, S. H., Zhang, A. L. and Zhan, X.X. (2017b), "Performance analysis and design of bolted connections in modularized prefabricated steel structures", *J. Constr. Steel Res.*, **133**, 360-373. https://doi.org/10.1016/j.jcsr.2017.02.025.

Liu, X., Pu, S., Zhang, A., Xu, A., Ni, Z., Sun, Y. and Ma, L. (2015), "Static and seismic experiment for bolted-welded joint in modularized prefabricated steel structure", *J. Constr. Steel Res.*, **115**, 417-433. https://doi.org/10.1016/j.jcsr.2015.08.036.

Liu, X., Yang, Z., Wang, H., Zhang, A., Pu, S., Chai, S. and Wu, L. (2017a), "Seismic performance of H-section beam to HSS column connection in prefabricated structures", *J. Constr. Steel Res.*, **138**, 1-16. https://doi.org/10.1016/j.jcsr.2017.06.029.

Mirghaderi, S., Torabian, S. and Keshavarzi, F. (2010), "I-beam to box-column connection by a vertical plate passing through the column", *Eng. Struct.*, **32**(8), 2034-2048. https://doi.org/10.1016/j.engstruct.2010.03.002.

Piluso, V. and Rizzano, G. (2008), "Experimental analysis and modelling of bolted T-stubs under cyclic loads", *J. Constr. Steel Res.*, **64**(6), 655-669. https://doi.org/10.1016/j.jcsr.2007.12.009.

Popov, E. and Takhirov, M. (2002), "Bolted large seismic steel beam-to-column connections Part 1: Experimental study", *Eng. Struct.*, **24**(12), 1523-1534. https://doi.org/10.1016/s0141-0296(02)00086-x.

Prinz, G., Nussbaumer, A., Borges, L. and Khadka, S. (2014), "Experimental testing and simulation of bolted beam-column connections having thick extended endplates and multiple bolts per row", *Eng. Struct.*, **59**, 434-447. https://doi.org/10.1016/j.engstruct.2013.10.042.

Shahidi, F., Rezaeian, A., Jamal-Omidi, M. and Shahidi, F. (2014), "Investigation of the ConXL moment connection cyclic behavior in box columns without filling concrete with different arrangement of collar bolts", *Struct. Des. Tall Spec. Build.*, **24**(5), 317-350. https://doi.org/10.1002/tal.1167.

Shi, Y., Shi, G. and Wang, Y. (2007), "Experimental and theoretical analysis of the moment-rotation behaviour of stiffened extended end-plate connections", *J. Constr. Steel Res.*, **63**(9), 1279-1293. https://doi.org/10.1016/j.jcsr.2006.11.008.

Swanson, J. and Leon, R. (2000), "Bolted steel connections: Tests on T-stub components", *J. Struct. Eng.*, **126**(1), 50-56. . https://doi.org/10.1061/(asce)0733-9445(2000)126:1(50).

Wang, J., Zhang, N. and Guo, S. (2016), "Experimental and numerical analysis of blind bolted moment joints to CFTST columns", *Thin-Walled Struct.*, **109**(5), 185-201. https://doi.org/10.1016/j.tws.2016.07.017.

Xue, J., Qi, L., Yang, K. and Wu, Z. (2017), "Dynamic experimental study on single and double beam column joints in steel traditional-style buildings", *Struct. Eng. Mech.*, **63**(5), 617-628. https://doi.org/10.12989/sem.2017.63.5.617.

PL